

Improvement of the low-field-induced magnetocaloric effect in $EuTiO_3$ compounds

Shuang Zeng(曾爽)[1], Wen-Hao Jiang(姜文昊)[1], Hui Yang(杨慧)[1], Zhao-Jun Mo(莫兆军)[1,†] Jun Shen(沈俊)[2,‡], and Lan Li(李岚)[1]

Citation: Chin. Phys. B, 2020, 29 (**12**): 127501. DOI: 10.1088/1674-1056/abb230
Journal homepage: http://cpb.iphy.ac.cn; http://iopscience.iop.org/cpb

What follows is a list of articles you may be interested in

Table-like shape magnetocaloric effect and large refrigerant capacity in dual-phase $HoNi/HoNi_2$ composite

Dan Guo(郭丹), Yikun Zhang(张义坤), Yaming Wang(王雅鸣), Jiang Wang(王江), Zhongming Ren(任忠鸣)
Chin. Phys. B, 2020, 29 (**10**): 107502. DOI: 10.1088/1674-1056/aba9be

Metamagnetic transition and reversible magnetocaloric effect in antiferromagnetic DyNiGa compound

Yan-Hong Ding(丁燕红), Fan-Zhen Meng(孟凡振), Li-Chen Wang(王利晨), Ruo-Shui Liu(刘若水), Jun Shen(沈俊)
Chin. Phys. B, 2020, 29 (**7**): 077501. DOI: 10.1088/1674-1056/ab90f3

Multicaloric and coupled-caloric effects

Jia-Zheng Hao(郝嘉政), Feng-Xia Hu(胡凤霞), Zi-Bing Yu(尉紫冰), Fei-Ran Shen(沈斐然), Hou-Bo Zhou(周厚博), Yi-Hong Gao(高怡红), Kai-Ming Qiao(乔凯明), Jia Li(李佳), Cheng Zhang(张丞), Wen-Hui Liang(梁文会), Jing Wang(王晶), Jun He(何峻), Ji-Rong Sun(孙继荣), Bao-Gen Shen(沈保根)
Chin. Phys. B, 2020, 29 (**4**): 047504. DOI: 10.1088/1674-1056/ab7da7

Magnetocaloric effect and critical behavior of the Mn-rich itinerant material Mn_3GaC with enhanced ferromagnetic interaction

Pengfei Liu(刘鹏飞), Jie Peng(彭杰), Mianqi Xue(薛面起), Bosen Wang(王铂森)
Chin. Phys. B, 2020, 29 (**4**): 047503. DOI: 10.1088/1674-1056/ab7da1

Giant low-field magnetocaloric effect in $EuTi_{1-x}Nb_xO_3$ (x=0.05, 0.1, 0.15, and 0.2) compounds

Wen-Hao Jiang(姜文昊), Zhao-Jun Mo(莫兆军), Jia-Wei Luo(罗佳薇), Zhe-Xuan Zheng(郑哲轩), Qiu-Jie Lu(卢秋杰), Guo-Dong Liu(刘国栋), Jun Shen(沈俊), Lan Li(李岚)
Chin. Phys. B, 2020, 29 (**3**): 037502. DOI: 10.1088/1674-1056/ab69e7

Improvement of the low-field-induced magnetocaloric effect in $EuTiO_3$ compounds*

Shuang Zeng(曾爽)[1], Wen-Hao Jiang(姜文昊)[1], Hui Yang(杨慧)[1], Zhao-Jun Mo(莫兆军)[1,†] Jun Shen(沈俊)[2,‡], and Lan Li(李岚)[1]

[1] School of Material Science and Engineering, Institute of Material Physics, Key Laboratory of Display Materials and Photoelectric Devices of Ministry of Education, Key Laboratory for Optoelectronic Materials and Devices of Tianjin, Tianjin University of Technology, Tianjin 300191, China

[2] Key Laboratory of Cryogenics, Technical Institute of Physics and Chemistry, Chinese Academy of Sciences, Beijing 100190, China

(Received 15 May 2020; revised manuscript received 12 August 2020; accepted manuscript online 25 August 2020)

The magnetocaloric effect of Mn, Ni, and Mn–Ni-doped $EuTiO_3$ compounds are studied in the near-liquid-helium-temperature range. The $Eu(Ti_{0.9375}Mn_{0.0625})O_3$, $Eu(Ti_{0.975}Ni_{0.025})O_3$, and $Eu(Ti_{0.9125}Mn_{0.0625}Ni_{0.025})O_3$ are prepared by the sol–gel method. The $Eu(Ti_{0.9375}Mn_{0.0625})O_3$ and $Eu(Ti_{0.9125}Mn_{0.0625}Ni_{0.025})O_3$ exhibit ferromagnetism with second-order phase transition, and the $Eu(Ti_{0.975}Ni_{0.025})O_3$ displays antiferromagnetic behavior. Under the magnetic field change of 10 kOe (1 Oe = 79.5775 $A{\cdot}m^{-1}$), the values of magnetic entropy change are 8.8 $J{\cdot}kg^{-1}{\cdot}K^{-1}$, 12 $J{\cdot}kg^{-1}{\cdot}K^{-1}$, and 10.9 $J{\cdot}kg^{-1}{\cdot}K^{-1}$ for $Eu(Ti_{0.9375}Mn_{0.0625})O_3$, $Eu(Ti_{0.975}Ni_{0.025})O_3$, and $Eu(Ti_{0.9125}Mn_{0.0625}Ni_{0.025})O_3$, respectively. The co-substitution of Mn and Ni can not only improve the magnetic entropy change, but also widen the refrigeration temperature window, which greatly enhances the magnetic refrigeration capacity. Under the magnetic field change of 10 kOe, the refrigerant capacity value of $Eu(Ti_{0.9125}Mn_{0.0625}Ni_{0.025})O_3$ is 62.6 $J{\cdot}kg^{-1}$ more than twice that of $EuTiO_3$ (27 $J{\cdot}kg^{-1}$), indicating that multi-component substitution can lead to better magnetocaloric performance.

Keywords: magnetocaloric effect, magnetic entropy change, magnetic phase transformation

PACS: 75.30.Sg, 65.40.gd, 75.30.Kz **DOI:** 10.1088/1674-1056/abb230

1. Introduction

Cryogenic technology is widely used in cutting-edge scientific research fields for providing extreme environment and greatly improving the resolution and signal-to-noise ratio of detection instruments. It may be used everywhere, including space detection, scientific research, and military fields. In recent years, based on the magnetocaloric effect (MCE),[1] magnetic refrigeration (MR) has attracted much attention for its advantages of environmental friendliness, energy saving, and high efficiency. Isothermal magnetic entropy change (ΔS_M) and refrigerant capacity (RC) are important parameters, which can quantitatively characterize the MCE performance. The MR technology does not rely on gravity nor scarce working fluids (^{3}He and ^{4}He), and it has become one of the significant technologies in terms of low temperature refrigeration.[2]

In the research of magnetocaloric effects, the study on rare earth metal oxides has become a hot research topic. As a rare earth titanate ($ReTiO_3$), $EuTiO_3$ (ETO) has a coupling effect between spin and charge ordering, and the spin magnetic moment is 7/2.[3–6] The permittivity of the G-type antiferromagnetic (AFM) significantly reduces 5.6 K, suggesting a larger magnetoelectric coupling.[7–9] The ETO, a low-temperature magnetic refrigeration material, has a large ΔS_M in the liquid helium temperature region. What is more, the ferromagnetic (FM) state and AFM state can coexist in the ETO, but the magnetization state is easily affected by experimental method. Therefore, the dielectric, transport, and magnetic properties of ETO are easily adjusted by external means, such as strain, pressure, and chemical doping.[10] In recent years, the improvement of the magnetocaloric effect of ETO has been reported. A large number of studies revealed that B-site doping is a crucial mean to affect the magnetic properties of ETO.[10–16] The Nb-doped ETO presents the FM state and the value of maximal magnetic entropy (ΔS_M^{max}) reaches 14.7 $J{\cdot}kg^{-1}{\cdot}K^{-1}$ for the single crystal $EuTi_{0.85}Nb_{0.15}O_3$ under a magnetic field in a range of 0 kOe–10 kOe.[13] Roy *et al.*[14] discovered that $EuTi_{0.9}V_{0.1}O_3$ has a large ΔS_M^{max} of 20 $J{\cdot}kg^{-1}{\cdot}K^{-1}$ when the magnetic field changes from 0 kOe to 20 kOe. The $EuTi_{1-x}Al_xO_3$ compounds at $0.10 \le x \le 0.50$ display the FM insulation behaviors. At $0.10 \le x \le 0.33$, the Curie temperature T_C is around 4 K. When x increases from 0.33 to 1, T_C presents a downward trend.[15] The values of ΔS_M^{max} and RC are 15.6 $J{\cdot}kg^{-1}{\cdot}K^{-1}$ and 58.2 $J{\cdot}kg^{-1}$ for $EuTi_{0.85}Al_{0.15}O_3$, with magnetic field changing from 0 kOe to 10 kOe, respectively.[16] Therefore, the FM coupling and the magnetocaloric effect can be improved in the ETO.

*Project supported by the National Key Research and Development Program of China (Grant No. 2017YFB0702704), the National Natural Science Foundation of China (Grant Nos. 11504266 and 51676198), the Tianjin Natural Science Foundation, China (Grant No. 17JCQNJC02300), and the Science & Technology Development Fund of Tianjin Education Commission for Higher Education, China (Grant No. 2017KJ247).

†Corresponding author. E-mail: mzjmzj163@163.com

‡Corresponding author. E-mail: jsen@mail.ipc.ac.cn

© 2020 Chinese Physical Society and IOP Publishing Ltd

The multi-component doping often has an obvious effect on the improvement of material properties.[17–20] For example, Nd-doped $LaFe_{13-x}Si_x$ compounds could improve the value of ΔS_M because of the enhancement of itinerant electron magnetic transition. Owing to the improvement of Fe–Fe interaction and inhabitation of itinerant electron metamagnetic, co-doped $LaFe_{13-x}Si_x$ compounds could increase the transition temperature and reduce the hysteresis loss. When Nd and Co co-dope $LaFe_{13-x}Si_x$ compounds, not only can their T_C values be enhanced to room temperature, but also a large ΔS_M and a negligible hysteresis loss are still maintained.[20] The substitution of Mn for Ti improves the magnetic susceptibility and the substitution of Ni for Ti can give rise to large saturation magnetization in ETO compounds.[21,22] Therefore, in this work we report the magnetocaloric effect of B-site element that replaces Mn–Ni in $EuTiO_3$ compounds. The $Eu(Ti_{0.9375}Mn_{0.0625})O_3$ (ETMO), $Eu(Ti_{0.975}Ni_{0.025})O_3$ (ETNO), and $Eu(Ti_{0.9125}Mn_{0.0625}Ni_{0.025})O_3$ (ETMNO) are synthesized by the sol–gel method and their MCEs and refrigerant capacities are explored. The ETMNO displays a very high refrigerant capacity (62.6 $J{\cdot}kg^{-1}$), and multi-component doping presents some inspirations for discovering more suitable magnetic refrigeration materials.

2. Experimental details

The $Eu(Ti_{0.9375}Mn_{0.0625})O_3$, $Eu(Ti_{0.975}Ni_{0.025})O_3$, and $Eu(Ti_{0.9125}Mn_{0.0625}Ni_{0.025})O_3$ were synthesized by the sol–gel method. According to the stoichiometric ratio, europium oxide (Eu_2O_3) was dissolved in aqueous nitric acid solution, the resulting solution was stirred until it became clarified, and then added into by manganese acetate ($Mn(CH_3COO)_2{\cdot}4H_2O$). Afterwards, nickel chloride ($NiCl_2{\cdot}6H_2O$) was added into the solution. Tetrabutyl titanate (TBT) was dissolved in a certain amount of aqueous nitric acid and stirred, until it was completely dissolved. Then, the two solutions were mixed together, and an appropriate amount of ethylene glycol was added into the mixture and the mixture was stirred for 30 min. Subsequently, the mixed solution was dried in a drying box at 60 °C for 12 h, and then dried at 245 °C for 2 h. Next, the dried oxide was sufficiently ground for 1 h. The ground powder was sintered at 1000 °C for 3 h and then naturally cooled at room temperature and was ground again for 1 hour. Finally, the power sample was placed in a tube furnace and sintered at 1200 °C in H_2–Ar mixture (1:10) for 3 h to obtain a desired experiment sample.

The structures of the compounds $Eu(Ti_{0.9375}Mn_{0.0625})O_3$, $Eu(Ti_{0.975}Ni_{0.025})O_3$, and $Eu(Ti_{0.9125}Mn_{0.0625}Ni_{0.025})O_3$ were investigated by a Rigaku 2500/PC x-ray diffractometer with a Cu-$K\alpha$ radiation source, whose wavelength was 1.54184 Å. The magnetization (M) changing with temperature (T) was measured by a commercial superconducting quantum interference device (SQUID) magnetometer. The Oxygen content was measured by an oxygen nitrogen analyzer (leco, TC500).

3. Results and discussion

The ETO has a cubic perovskite structure with $Pm3m$ space group near room temperature with a lattice parameter of 3.905 Å.[7] Figure 1 illustrates the x-ray diffraction patterns of the samples at room temperature. The diffraction peak for each of samples corresponds to the ETO standard spectrum, and no impurity is found within the resolution of x-ray diffractometer, indicating that each sample is of pure phase and possesses a cubic perovskite structure. There exists no obvious shift happening to these diffraction peaks, because the ionic radius of Mn^{2+} ($\sim$ 0.67 Å) and Ni^{2+} ($\sim$ 0.69 Å) are similar to Ti^{4+} ($\sim$ 0.61 Å). According to valence equilibrium, it is inevitable to generate the oxygen vacancy defect or Eu^{3+}. The values of oxygen content of ETNO, ETMO, and ETMNO are 19.3%, 19.2%, and 19.2%, respectively, suggesting the existence of oxygen vacancies and Eu^{3+} ions.

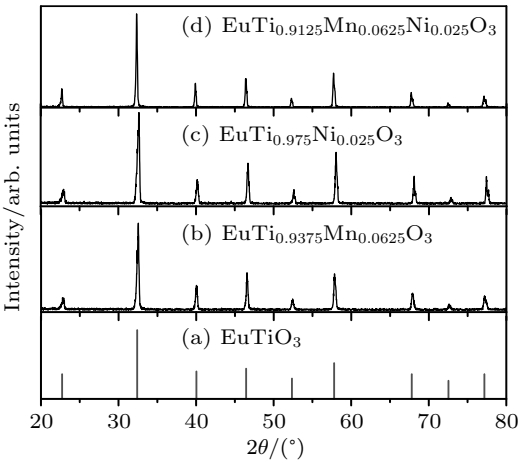


Fig. 1. XRD patterns of (a) ETO, (b) ETMO, (c) ETNO, and (d) ETMNO at room temperature.

Figure 2 shows the temperature dependence of the magnetization (M–T) in heating (black symbol) and cooling (red symbol) process for ETMO (Fig. 2(a1)), ETNO (Fig. 2(a2)) and ETMNO (Fig. 2(a3)). In the heating process, M–T measurements are performed at field $H = 100$ Oe and in temperature range from 3 K to 300 K. The samples are cooled to 3 K in the presence of $H = 100$ Oe to obtain the M–T data of cooling process. Distinctly, the heating curves basically coincide with the cooling curves as shown in Figs. 2(a1) and 2(a2). It means that ETMO and ETNO compounds scarcely have the thermal hysteresis around transition temperature, which is good for the heat exchange. Here the magnetic transition temperature is determined by the peak value of dM/dT. The inset of Fig. 2(b1) displays two consecutive magnetic transitions for ETMO compounds with the increase of temperature at the corresponding low-temperature peaks in the (dM/dT)–T curve. The first anomaly around spin transition temperature $T_t = 5$ K is con-

sidered to be a transition from collinear to non-collinear magnetic structure.[23] The second change $T_C = 9.5$ K originates from the FM to paramagnetic (PM) state transition. The first abnormality at lower temperature may come from magnetic frustration and the other change of magnetization around Néel temperature $T_N = 5.5$ K is the magnetic transition from AFM to PM states (the inset of Fig. 2(b2). The $EuTi_{1-x}Ni_xO_3$ compound exhibited AFM behavior when $x < 0.1$ in our previous reports.[22] This cusp feature of M–T curve results from the G-type AFM transition at ~ 5 K that is induced by Eu^{2+} spins ordering below T_N.[7,24,25] As shown in Fig. 2(a3), for ETMNO compound, the difference between the heating curve and cooling curve can be observed below 5 K. The magnetic frustration behavior or a spin-glass-like surface layer could cause spike-like peaks in the heating time.[26] Perhaps, the differences between the temperature-rising curves and the cooling curves are ascribed to the certain inherent magnetic moment of Mn and Ni ions, which can lead to a magnetic frustration behavior. The inset of Fig. 2(b3) clearly shows an FM–PM transition that occurs about 7 K. Part of Ti elements are replaced by Nb, Zr, Al, and other elements affects the magnetic exchange (Eu 4f–Ti 3d–Eu 4f) and adjusts the transition temperature such as in $EuTi_{1-x}Nb_xO_3$, $EuTi_{1-x}Zr_xO_3$, $EuTi_{1-x}Sc_xO_3$, $EuTi_{1-x}Al_xO_3$, and $EuTi_{1-x}Cr_xO_3$.[20,25,27–30]

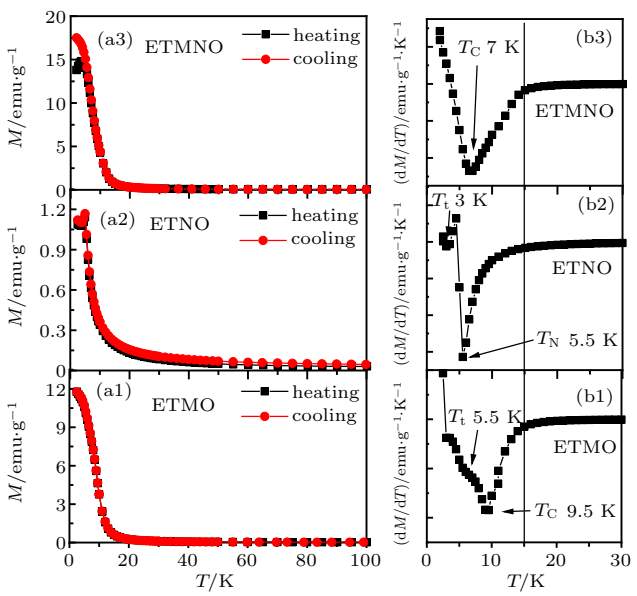


Fig. 2. Plots of magnetization (M) *versus* temperature under heating and cooling for (a1) ETMO, (a2) ETNO, and (a3) ETMNO, respectively. Plots of (dM/dT)–T for (b1) ETMO, (b2) ETNO, (b3) ETMNO.

In order to investigate the effects of substitution on magnetic performance, the isothermal magnetization M–H curves are measured in a temperature from 3 K to 28 K for ETMO, ETNO, and ETMNO as illustrated in Figs. 3(a), 3(b), and 3(c), respectively. The ETMO and ETMNO show that their magnetizations sharply increase at low field and trend to be saturated with the increase of the field as shown in Figs. 3(a) and 3(c), which is the typical nature of FM material. The field dependence of the magnetization reveals a linear relationship (PM state) because the temperature is higher than 20 K. When the temperature is between T_C and 18 K, the field dependence of the magnetization is nonlinear, proving that there are some short-range ferromagnetic clusters in the PM state. Figure 3(b) exhibits representative isothermal magnetization curves at the temperature ranging from 3 K to 28 K for ETNO. At low magnetic field (< 6 kOe), the M increases almost linearly, followed by a saturating trend close to 10 kOe. The field-induced transition from AFM to FM is not observed clearly, so maybe it needs a very small magnetic field to trigger the magnetic transition between AFM state and FM state which are co-existent in ETO compounds. Generally, the G-type AFM states of ETO compounds are not very stable. Eu^{2+} spins have Heisenberg characteristics and weak magnetic anisotropy. Under the field action, Heisenberg spins are sorted by AFM state immediately and flip to an arrangement perpendicular to H and gradually transit into the FM arrangement when the field increases.[27] Figure 3(d) exhibits the isothermal magnetization curves of compounds at $T = 3$ K. By comparison, the ETMNO not only has large saturation magnetization, but also exhibits large magnetic susceptibility, which refers to a small saturation field and a larger saturation magnetization. The value of M for ETMO and ETMNO are much larger than that for ETNO under low magnetic field (< 10 kOe). In our previous report,[21] Mn^{2+} and Mn^{4+} can coexist when Mn is doped. The magnetic moments of Mn^{2+} (5 μ_B) may be antiparallel to that of the Eu^{2+} ions, and Mn^{2+} ions can cause the change from Eu^{2+} to Eu^{3+} (no magnetic moment) for the valence equilibrium, so the total magnetic moment decreases. When a small number of Ni^{2+} ions are added, the number of Mn^{2+} ions decreases because of the valence equilibrium, so a large magnetic moment is created. Magnetic hysteresis loops of ETMO, ETNO, and ETMNO are measured at 3 K, which exhibits the negligible coercivity. The existence of neither magnetic hysteresis nor thermal hysteresis of magnetization is favorable for their applications in magnetic refrigeration.

The ΔS_M can be calculated by isothermal magnetic data based on Maxwell relation

$$\Delta S_M = \int_0^H \left(\frac{\partial M(H,T)}{\partial T}\right)_H \mathrm{d}H.$$

The temperature dependence of ΔS_M of magnetic field between 10 kOe and 50 kOe for ETMO, ETNO, and ETMNO compounds are presented in Figs. 4(a)–4(c). The temperature that corresponds to ΔS_M^{max} increases from 4.5 K ($\Delta H =$ 10 kOe) to 5.5 K ($\Delta H = 50$ kOe) with the increase of the magnetic field for ETMO and ETMNO compounds, indicating a typical FM feature. For the ETNO compound, the temperature that corresponds to ΔS_M^{max} declines from 5.5 K ($\Delta H = 10$ kOe) to 4.5 K ($\Delta H = 50$ kOe), implying the AFM nature of ETNO compound. The maximum values of ΔS_M ($-\Delta S_M^{max}$) are 31.3 J·kg^{-1}·K^{-1} (ETMO), 42.2 J· kg^{-1}·K^{-1}

(ETNO), and 33.1 J· kg^{-1}·K^{-1} (ETMNO) for a field change of 0 kOe–50 kOe. Figure 4(d) gives the values of $\Delta S_{\rm M}$ for the substituted samples under $\Delta H = 10$ kOe, in which the $\Delta S_{\rm M}$ of ETO is taken as a reference. For the ETMO compound, although the value of $\Delta S_{\rm M}^{\rm max}$ (8.8 J·kg^{-1}·K^{-1}) is smaller than that of ETO compound (9.8 J·kg^{-1}·K^{-1}) for its lower saturation magnetization, the values of $\Delta S_{\rm M}$ are larger than those of ETO except those in the surrounding area of transition temperature, for the two magnetic transitions exist. For the ETNO compound, the value of $\Delta S_{\rm M}^{\rm max}$ (12 J·kg^{-1}·K^{-1}) is larger than that of ETO compound, and the values of $\Delta S_{\rm M}$ are larger than those of ETO compound below 10 K, especially below transition temperature. Perhaps, it is attributed to the spin-glass at 3 K caused by magnetic frustration. The value of $\Delta S_{\rm M}$ for ETMNO compound is larger than that of ETO in a temperature range from 3 K to 28 K.

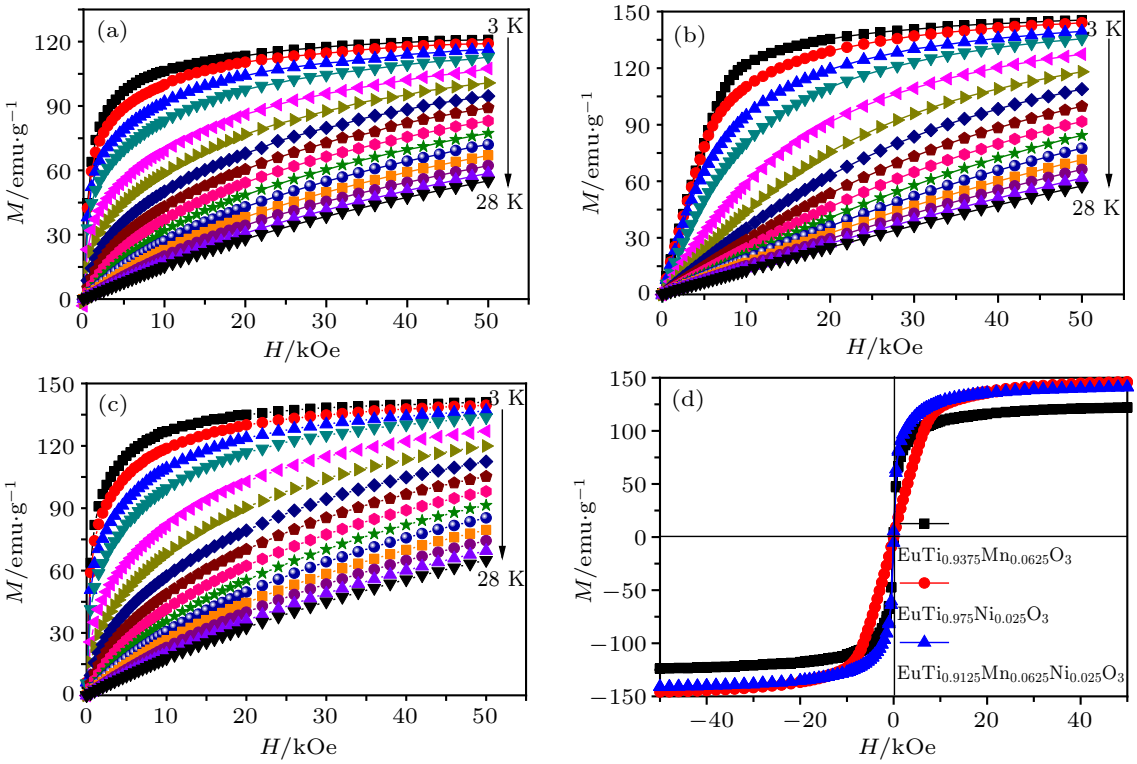


Fig. 3. Plots of magnetization (M) *versus* magnetic field (increasing only) for (a) ETMO, (b) ETNO, and (c) ETMNO at some selected temperatures, and (d) magnetization curves of ETMO, ETNO, and ETMNO at 3 K.

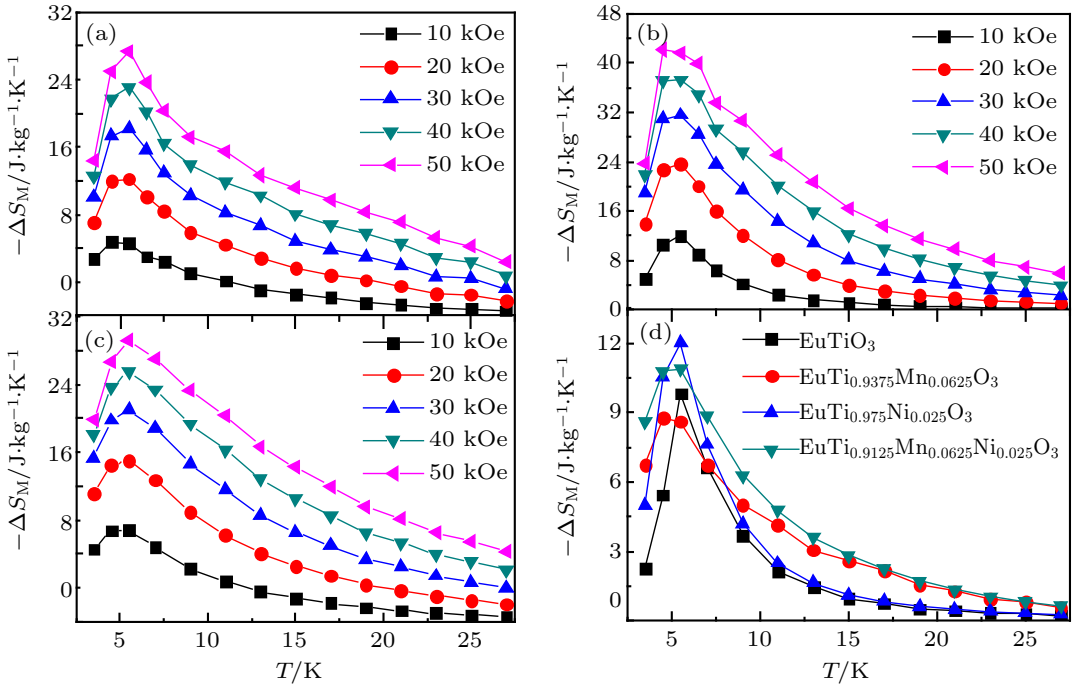


Fig. 4. Plots of values of $\Delta S_{\rm M}$ *versus* temperature for various values of magnetic field change ΔH up to 10 kOe–50 kOe for (a) ETMO, (b) ETNO, and (c) ETMNO, respectively. (d) $\Delta S_{\rm M}$ *versus* temperature (T) for ETO, ETMO, ETNO, and ETMNO under $\Delta H = 10$ kOe.

The RC is considered as another important criterion for the performance of magnetic refrigerant materials. It reflects the amount of heat that transfers between cold storage and heat storage in an ideal refrigeration cycle. It is defined as $RC = \int_{T2}^{T1} \Delta S \mathrm{d}T$, where T_1 and T_2 denote the temperatures that correspond to both sides of the half value of the $\Delta S_{\mathrm{M}}^{\max}$. When the magnetic field changes from 0 kOe to 10 kOe, the RC values are 49.2 J·kg^{-1}, 37.6 J·kg^{-1} and 62.6 J·kg^{-1} for ETMO, ETNO, and ETMNO, respectively, which are all larger than that of ETO. Especially, the RC value of ETMNO is twice more than that of ETO (27 J·kg^{-1}), which is ascribed to the higher ΔS_{M} and wider temperature window.

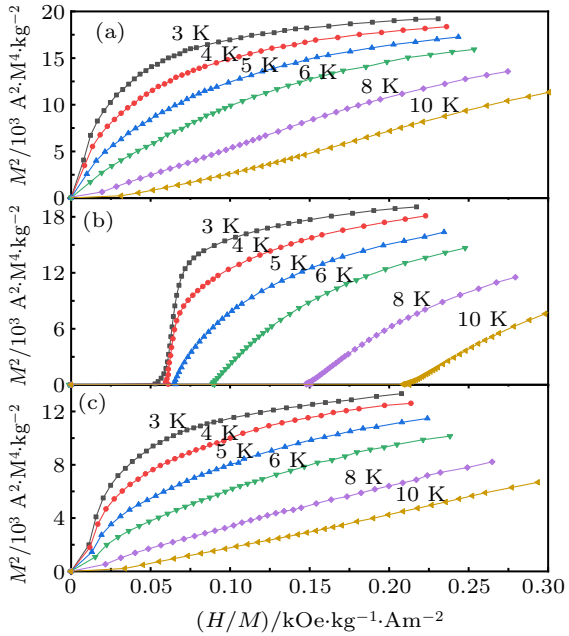


Fig. 5. Plots of (H/M) *versus* M^2 for (a) ETMO, (b) ETNO, and (c) ETMNO at some selected temperatures.

The phase transition of materials includes the first-order phase transition and the second-order phase transition. The first-order phase transition is strongly coupled with the magnetic and structural transition, which leads to a larger ΔS_{M}.[31–33] However, the thermal hysteresis, magnetic hysteresis and mechanical instability are the disadvantages that limit the practical applications of the first-order phase transition system. Whereas, the magnetic hysteresis and thermal hysteresis are almost negligible in the second-order phase transition.[34] Meanwhile, the second-order phase transition compounds have better mechanical stability, which makes them more suitable for magnetic refrigeration. Figure 5 shows the Arrott plots of ETMO, ETNO, and ETMNO compounds for clarifying the properties of magnetic transitions. According to Banerjee criterion, the first-order phase transition displays the negative slope of the curve and the second-order phase transition shows positive slopes.[35,36] As shown in Figs. 5(a) and 5(c), both ETMO compound and ETMNO compound have the second-order nature. For the ETNO compound, a negative slope can be observed in the Arrott curve around transition temperature. Figure 5(b) reveals that the magnetic transition is from AFM to PM state. In addition, the types of phase transitions of these materials can also be seen by overlapping the $\Delta S'(\theta)$ curves as shown in Fig. 6. The curves of ETMO and ETMNO (Figs. 6(a) and 6(c)) are overlapped well, which further proves that each of them experiences the second-order phase transition. However, the curves of ETNO compound are discrete in Fig. 6(b), which may be caused by the AFM of ETNO.

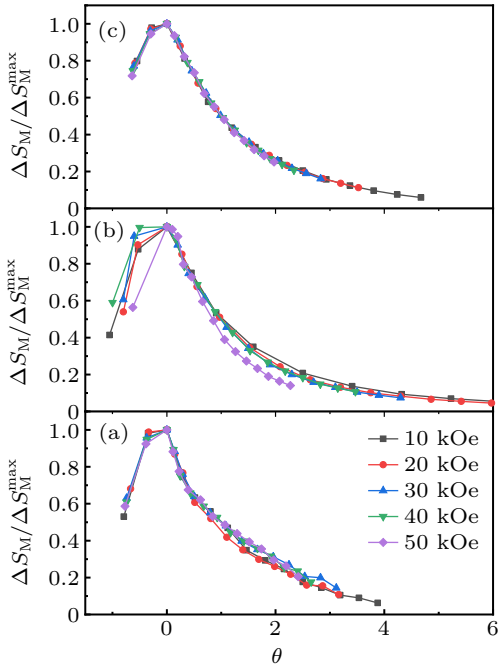


Fig. 6. Curves of θ-dependent $\Delta S'(T)$ for typical field changes in (a) ETMO, (b) ETNO, (c) ETMNO compounds.

4. Conclusions

The ETMNO compound is synthesized by doping Mn and Ni into $EuTiO_3$ compound. It exhibits ferromagnetic behavior and a giant magnetocaloric effect under a low magnetic field change. When the magnetic field changes from 0 kOe to 10 kOe, the value of $\Delta S_{\mathrm{M}}^{\max}$ reaches 10.9 J·kg^{-1}·K^{-1} that is larger than that of the $EuTiO_3$ (9.8 J·kg^{-1}·K^{-1}). Meanwhile, the cooling temperature window becomes wider, so the RC value of ETMNO is twice more than that of ETO. The improvement of magnetocaloric performance is attributed to the enhancement of ferromagnetic coupling. Most importantly, ETMNO belongs to the second-order phase transition with minimal thermal hysteresis and hysteresis and is one of the materials suitable for practical applications in magnetic refrigeration.

References

[1] Li L W and Yan M 2020 *J. Alloys Compd.* **823** 153810
[2] Zhang H, Gimaev R, Kovalve B, Kamilov K, Zverev V and Tishin A 2019 *Phys. Rev. B* **558** 65
[3] Lee J H, Fang L, Vlahos E, *et al.* 2010 *Nature* **466** 954
[4] Shvartsman V V, Borisov P, Kleemann W, Kamba S and Katsufuji T 2010 *Phys. Rev. B* **81** 064426

[5] Hatabayashi K, Hitosugi T, Hirose Y, Cheng X Q, Shimada T and Hasegawa T 2009 *Jpn. J. Appl. Phys.* **48** 100208
[6] Kamba S, Nuzhnyy D, Vanek P, Savinov M, Knizek K, Shen Z, Santava E, Maca K, Sadowski M and Petzelt J 2007 *Europhys. Lett.* **80** 27002
[7] Wei T, Liu H P, Chen Y F, Yan H Y and Liu J M 2011 *Appl. Surf. Sci.* **257** 4505
[8] Scagnoli V, Allieta M, Walker H, Scavini M, Katsufuji T, Sagarna L, Zaharko O and Mazzoli C 2012 *Phys. Rev. B* **86** 094432
[9] McGuire T R, Shafer M W, Joenk R J, Halperin H A and Pickart S J 1966 *J. Appl. Phys.* **37** 981
[10] Xu S, Gu Y, Wu X S 2020 *J. Magn. Magn. Mater.* **497** 166077
[11] Wang X Y, Zhen S Q, Min Y, Zhou P X, Huang Y Y, Li J F, Chong C G and Dong Z C 2016 *J. Alloys Compd.* **689** 63
[12] Li L, Zhou H D, Yan J Q, Mandrus D and Keppen V 2014 *APL Mater.* **2** 110701
[13] Roy S, Khan N and Mandal P 2016 *APL Mater.* **4** 026102
[14] Roy S, Das M and Mandal P 2018 *Phys. Rev. Materials* **2** 064412
[15] Liu Y, Ivanovski N V and Petrovic C 2017 *Phys. Rev. B* **96** 184419
[16] Zhang W, Mo Z J, Jiang W H, Hao Z H, Luo J W, Cheng R J, Liu G D, Li L and Shen J 2019 *J. Magn. Magn. Mater.* **492** 165684
[17] Li L, Han E S, Zhu L Z, Qiao S P, Du C Y and Liu H 2020 *Solid State Ionics* **346** 115220
[18] Maarouf M and Al-Sunaidi A 2020 *Comput. Theor. Chem.* **1175** 112728
[19] Ma J N, Lin J Y, Liu J Y, Li F, Liu Y C and Yang G C 2020 *Chem. Phys. Lett.* **746** 137308
[20] Shen J, Li Y X, Zhang J, Guo B, Hu F X, Zhang H W, Chen Y Z, Rong C B and Sun J R 2008 *J. Appl. Phys* **103** 07B317
[21] Mo Z J, Sun Q L, Shen J, Wang C H, Meng F B, Zhang M H, Huo Y, Li L and Liu G D 2018 *J. Alloys Compd.* **753** 1
[22] Mo Z J, Jiang W H, Zhao Y, Hao Z H, Zheng Z X, Zhang W, Li L and Shen J 2019 *J. Magn. Magn. Mater.* **477** 258
[23] Zhang H, Xu Z Y, Zheng X Q, Shen J, Hu F X, Sun J R and Shen B G 2011 *J. Appl. Phys.* **109** 123926
[24] Katsufuji T and Tkagi H 2001 *Phys. Rev. B* **64** 054415
[25] Wei T, Song Q G, Zhou Q J, Li Z P, Qi X L, Liu W P, Guo Y R and Liu J M 2011 *Appl. Surf. Sci.* **258** 599
[26] Kodama R H, Berkowitz A E, McNiff E J Jr and Foner S 1996 *Phys. Rev. Lett.* **77** 394
[27] Mo Z J, Hao Z H, Shen J, Li L, Wu J F, Hu F X, Sun J R and Shen B G 2015 *J. Alloys Compd.* **649** 674
[28] Akahoshi D, Miyamoto G, Hayakawa Y and Satio T 2019 *J. Solid State Chem.* **280** 120985
[29] Midya A, Rubi Km, Chaudhuri A, Rusydi A and Mahendiran R 2019 *Solid State Commun.* **293** 33
[30] Li L, Zhou H D, Yan J Q, Mandrus D and Keppens V 2014 *APL Mater.* **2** 110701
[31] Wada H and Tanabe Y 2001 *Appl. Phys. Lett.* **79** 3302
[32] Liu J, Gottschall T, Skokov K P, Moore J D and Gutfleisch O 2012 *Nat. Mater.* **11** 620
[33] Choudhury D, Suzuki T, Okuyama D, Morikawa D, Kato K, Takata M, Kobayashi K, Kumai R, Nakao H, Murakami Y, Bremholm M, Iversen B B, Arima T, Tokura Y and Taguchi Y 2014 *Phys. Rev. B* **89** 104427
[34] Phan M and Yu S 2007 *J. Magn. Magn. Mater.* **308** 325
[35] Baneriee B 1964 *Phys. Lett.* **12** 16
[36] Arrott A 1957 *Phys. Rev.* **108** 1394